EPJ Web of Conferences **31**, 00032 (2012)
DOI: 10.1051/epjconf/20123100032
© Owned by the authors, published by EDP Sciences - SIF, 2012

KRATTA, a triple telescope array for charged reaction products

J. Łukasik[1], P. Pawłowski[1], A. Budzanowski[1,†], B. Czech[1], I. Skwirczyńska[1], J. Brzychczyk[2], M. Adamczyk[2], S. Kupny[2], P. Lasko[2], Z. Sosin[2], A. Wieloch[2], M. Kiš[3], Y. Leifels[3] and W. Trautmann[3]

[1] Institute of Nuclear Physics, IFJ-PAN, 31-342 Kraków, Poland
[2] Institute of Physics, Jagiellonian University, 30-059 Kraków, Poland
[3] GSI, D-64291 Darmstadt, Germany

Abstract

KRATTA, a new, low threshold, broad energy range triple telescope array has been built to measure the energy, emission angles and isotopic composition of light charged reaction products. It has been equipped with fully digital chains of electronics. The array performed very well during the ASY-EOS experiment, conducted in May 2011 at GSI. The structure and performance of the array are presented using the first experimental results.

1 Motivation and requirements

The construction of a novel detection system, KRATTA, KRAkow Triple Telescope Array, has been motivated mainly by the needs of the ASY-EOS experiment [1]. The experiment has been designed to study the density dependence of the nuclear symmetry energy by measuring flows and isotopic composition of the reaction products from the ^{197}Au+^{197}Au, ^{96}Ru+^{96}Ru and ^{96}Zr+^{96}Zr reactions at 400 MeV/nucleon. During the experiment the

[†]Deceased.

This is an Open Access article distributed under the terms of the Creative Commons Attribution License 2.0, which permits unrestricted use, distribution, and reproduction in any medium, provided the original work is properly cited.

Article available at http://www.epj-conferences.org or http://dx.doi.org/10.1051/epjconf/20123100032

most relevant products, neutrons and Z=1 and 2 particles, have been measured by the LAND [2] detector and the orientation and magnitude of the impact vector were estimated using the CHIMERA [3] and ALADIN ToF-Wall [4] detectors. The KRATTA array has been designed to provide a complementary to LAND information on isotopic composition and flow of light charged reaction products ($1 \leq Z \lesssim 7$), and specially, to identify the hydrogen and helium isotopes with a resolution much better than achievable with LAND. The array was placed on the opposite side of the beam with respect to LAND, and covered approximately the same solid angle (160 msr). Modular design, portability, low thresholds (below 3 MeV/nucleon) and high maximum energy ($\sim$260 MeV/nucleon for p and α), allow the array to be used in various configurations and experiments. In particular, it will very well suit the needs of the future cyclotron facility at IFJ-PAN in Kraków, planned for the proton beams from 70 to 250 MeV.

2 Active elements and geometry

The modules of KRATTA are composed of two CsI(Tl) crystals [5] and of three large area HAMAMATSU PIN photodiodes for direct detection [6]. The layout and dimensions of these active elements are presented in Fig. 1 and their main characteristics are summarized in table 1.

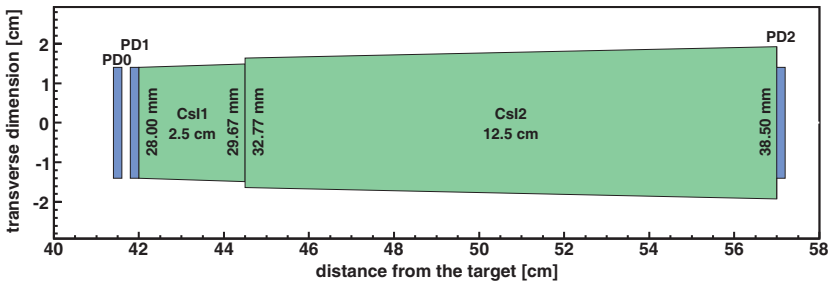

Figure 1: Schematic layout of the active elements of the module.

The first photodiode (PD0 in Fig. 1) serves as a Si ΔE detector providing the ionization signal alone. It has been "reverse mount", i.e. the ohmic side towards the incoming particles. The second photodiode (PD1), naturally "reverse mount", works in a "Single Chip Telescope", SCT [7], configuration and provides a combined signal composed of a direct (ionization) component and of a light output (LO) from the thin scintillator (CsI1). The third photodiode (PD2) reads out the light from the thick crystal (CsI2).

Table 1: Main characteristics of the active elements

Photodiodes [6]		CsI(Tl) Crystals [5]	
Active Area	28×28 mm^2	Tl concentration	1500 ppm
Thickness	500±15 μm	LO non-uniformity	< 7 %
Dead Layers	1.5 μm front	Shape	Truncated pyramids
	20 μm rear		
Full Depletion	120-135 V	Tolerance	±0.1 mm
Dark Current	6-16 nA	Wrapping [8]	
Rise Time	40 ns	Reflectance	> 98 %
Capacitance	190±3 pF	Thickness	65 μm

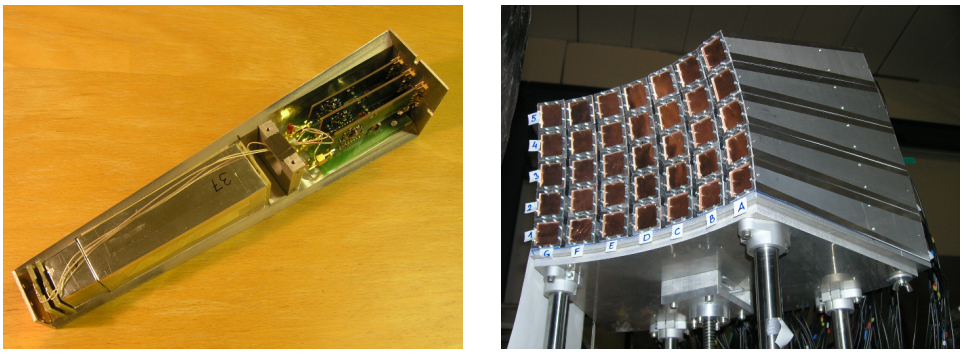

Figure 2: Left: single module content. Right: KRATTA in a 7×5 configuration.

The crystals have been polished and wrapped with a highly reflective ESR [8] foil, except for the front and back windows. The windows have been protected with 6 μm Mylar foils. The crystals were optically decoupled. The photodiode chips have been glued onto the custom-made PCB frames and put in close optical contact with the crystal windows. The active elements have been placed inside aluminum boxes together with the charge preamplifiers (see Fig. 2, left side). The PCB frames and the aluminum housing reduced the geometric acceptance of a single module to about 54%. The entrance window has been made of a 100 μm thick copper foil. During the experiment the 35 modules have been arranged in a 7×5 array (Fig. 2, right side). The energy thresholds for consecutive active layers of the triple telescope are summarized in table 2. As will be shown later on, the low threshold can be further reduced by applying a pulse shape analysis.

Fragment	E_{low}	E_{int}	E_{up}
^{1}H	8.3	100.5	266.0
^{4}He	8.3	100.3	265.5
^{7}Li	9.5	116.1	309.8
^{20}Ne	19.9	257.2	746.5
^{43}Ca	26.7	374.4	1170.9
^{91}Zr	34.0	557.9	1958.1
^{197}Au	38.6	824.4	3598.9

Table 2: Lower, E_{low}, intermediate, E_{int}, and upper, E_{up}, thresholds (in MeV/u) for selected species. The thresholds correspond to the energy losses in 500 μm of Si, in 1000 μm of Si + 2.5 cm of CsI and in 1000 μm of Si + 15 cm of CsI, respectively. The energy losses have been calculated using the ATIMA tables [9].

3 Electronics and data acquisition

The main electronics and data acquisition functions are presented schematically in Fig. 3. The photodiodes (3 per KRATTA module) have been reverse biased at 120 V, using the in-house made 120-channel, remote controlled, high voltage power supplies. The signal from each photodiode has been integrated with the own-design, low noise, charge preamplifier [10]. The resultant signal distortions, including the photodiode, electronics and pickup noise sources, have been observed on the level of 1 mV.

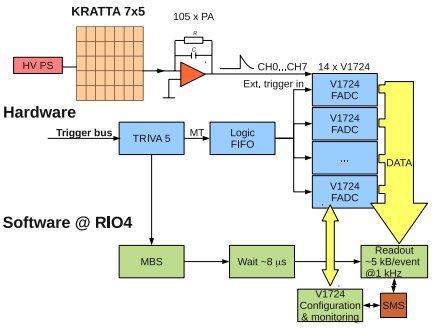

Figure 3: Analog, logical and digital signal flow chart. HV PS - high voltage power supply. PA - charge sensitive preamplifier. V1724 - CAEN digitizers. TRIVA5 - VME Trigger Synchronization Module [12]. MT - master trigger. FIFO - logical Fan-In Fan-Out module. RIO4 - VME controller board [13] running LynxOS. MBS - Multi Branch System, a GSI acquisition standard [14]. SMS - Shared Memory Segment.

The preamps were supplied with $\pm$6 V and their dynamic range spanned about 3.6 V. Three charge gains of the preamplifiers have been used, depending on the azimuthal angle of the module: 44.5, 22.2 and 13.5 mV/MeV, with the nominal fall time of 10 μs in each case. After optional amplification, the signals have been digitized with the 100 MHz, 14 bit digitizers [11] and stored for the off line analysis. All logical and digital electronics modules from Fig. 3 have been controlled with the RIO4 board [13] within a single VME crate. During the experiment the 14 Flash ADC boards have

been triggered with an external trigger split and delivered into each FADC module. The stored waveforms spanned 5.12 or 10.24 μs (512 or 1024 time bins), with a 2 μs pre-trigger enabling a precise baseline estimation. The shorter samples have been sufficient for the first photodiode supplying the fast ionization signal alone. The expected data throughput amounted to about 5 MB/s, assuming 1 kHz single hit rate. The actual data rate did not go beyond this estimate during the experiment. The digitizers have been remotely set up and monitored using a self-developed software. The data flow has been controlled using the standard GSI MBS system [14].

4 Pulse shape analysis

The following assumptions have been made to decompose the SCT output. The preamplifier response has been modeled using a simple parallel RC circuit assumption [15]: $\frac{dV(t)}{dt} + \frac{1}{RC}V(t) = \frac{i(t)}{C}$, where, RC is the feedback coupling constant, $i(t)$ is the induced current due to the carrier motion, and $V(t)$ is the measured voltage pulse. The induced current has been approximated with 3 ionization and 2 scintillation components of the form: $i_i(t) = Q_i \frac{t\, e^{-t/\tau_0}}{\tau_0^2}$ and $i_s(t) = Q_s \frac{e^{-t/\tau_1} - e^{-t/\tau_2}}{\tau_1 - \tau_2}$, respectively, where Q's are the induced charges and τ's are the rise and fall times for the respective component. The assumed shapes attempt to account for both, the complicated actual current pulse shape induced by the electrons and holes moving in the photodiode [16], and for the instrumental rise time of the preamp. The third ionization component, apart from the "electron" and "hole" ones, was introduced to improve the fit quality. The 2 scintillation components account for the fast and slow decay modes of the CsI(Tl) crystals. With these assumptions the model is analytically solvable and the resulting waveforms fit very well the measured ones. In the fitting procedure all the τ's have been kept constant, allowing to use a fast and efficient linear least squares method to calculate the 5 unknown amplitudes Q. An additional advantage of using the fitting method was the knowledge of the actual charges Q for each component despite the substantial ballistic deficit due to a relatively short fall time of the preamp ($RC \simeq 10$ μs). In the case of particles stopped in the first photodiode (PD0) the measured waveforms have been fitted using a single scintillation component, $i_s(t)$, which allowed for independent derivation of the rise and fall times and thus also of the position of the maximum (mode) of the current signal.

5 Performance

The reconstructed amplitudes for the first two and the last two layers of the KRATTA module are presented in Fig. 4. The ID map for the first 2 photodiodes (left panel) shows a complex spectrum with each "ID-line" composed of two parts: an ordinary Si-Si hyperbolic part at low energies, for particles stopped in PD1, and a more curved part for particles punching through the PD1 photodiode and stopped in the CsI1 crystal. The right panel of Fig. 4 shows a ΔE-E map for a second vs third photodiode. Apart from the very good isotopic resolution, one can see a substantial background from the secondary reactions/scatterings in the crystals and back-bendings corresponding to particles punching through the thick crystal.

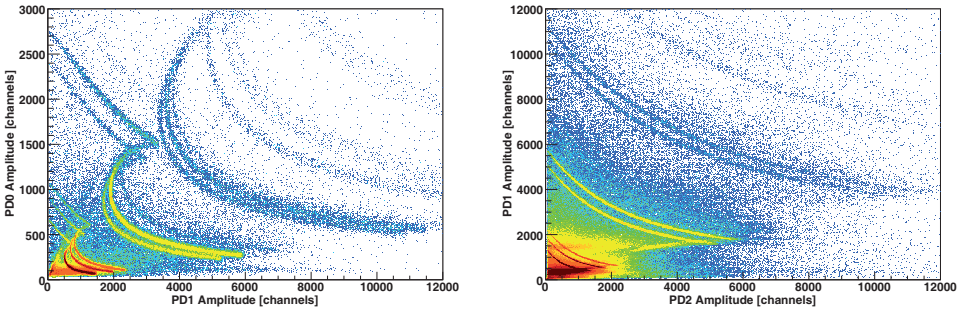

Figure 4: Raw ΔE-E identification maps for the triple telescope module. Left: PD0 vs PD1(SCT). Right: PD1(SCT) vs PD2.

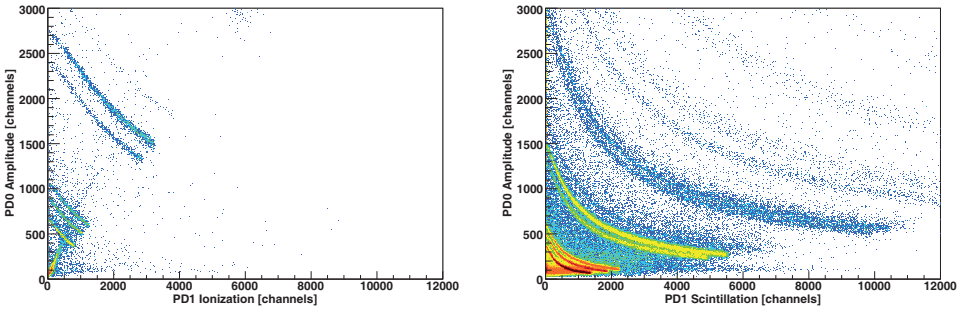

Figure 5: Decomposition of the map from the left panel of Fig. 4. Left: PD0 vs PD1(Si) - for particles stopped in PD1 and producing no light. Right: PD0 vs PD1(CsI) - for particles punching through PD1 and stopped in CsI1.

The strongest lines in Figs. 4-6 correspond to $p, d, t, ^3He, \alpha$, and so on, from bottom to top, respectively.

Using the individual reconstructed amplitudes for the ionization and for the scintillation components, the map from the left panel of Fig. 4 can be

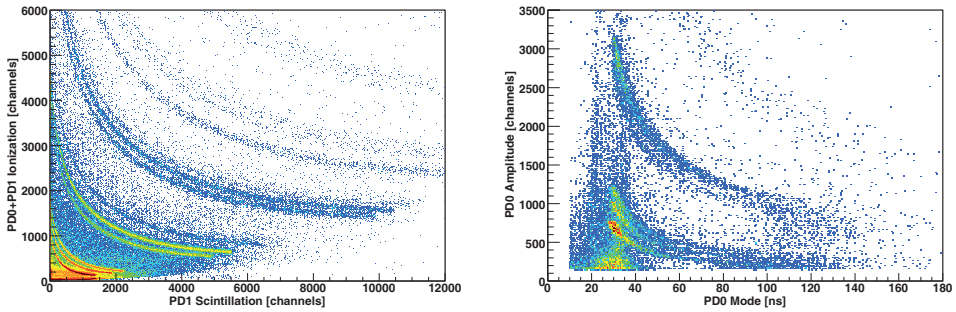

Figure 6: Left: Summed PD0+PD1 ionization components vs scintillation in PD1 for particles stopped in CsI1. To be compared with right panel of Fig. 5. Right: Amplitude vs mode of the current signal for particles stopped in PD0.

decomposed into Si-Si and Si-CsI components of the SCT segment (Fig. 5).

The resolution presented in the right panel of Fig. 5 can be sizably enhanced by summing up the ionization components from PD0 and PD1, and thus, increasing the effective thickness of the first ΔE layer to 1000 μm of Si (Fig. 6, left panel).

Pulse shape analysis allowed also to identify particles stopped in the first photodiode (Fig. 6, right panel). Due to the constant value of the field within the intrinsic region of the PIN diode the enhancement of the resolution for stopped particles is not expected to be as important as in the case of reverse mount PN detectors [17], nevertheless, the relation between the range and the charge collection time is still strong enough to enable the isotopic separation of light particles. This method allowed to reduce the lower identification threshold (see table 2) by about a factor of 3.

Summarizing, a new, low threshold, broad energy range, versatile array of triple telescopes, KRATTA, has been built and its performance presented. The modules, equipped with digital electronics chains, allowed for isotopic identification of light charged reaction products. The array has met the expectations and fulfilled the design requirements during the ASY-EOS experiment at GSI.

Acknowledgment

Work supported by Polish Ministry of Science and Higher Education under grant No. DPN/N108/GSI/2009.

Stimulating discussions, expertise and help of Giacomo Poggi as well as of Marian Pârlog, Remi Bougault and Hector Alvarez Pol during the design and test phase are greatly acknowledged.

References

[1] P. Russotto et al., contribution to these Proceedings; P. Russotto et al., IWM 2009, Conf. Proc. Vol. 101, p. 22; www.irb.hr/users/mkis; www.ct.infn.it/asyeos2010; P. Russotto et al., Phys. Lett. B 697 (2011) 471

[2] Th. Blaich et al., Nucl. Instr. Meth. A 314, 136 (1992)

[3] A. Pagano et al., Nucl. Phys. A 734 (2004) 504.

[4] A. Schuettauf et al., Nucl. Phys. A 607, 457 (1996)

[5] Manufacturer: Institute of Modern Physics, Chinese Academy of Sciences, Lanzhou, China

[6] HAMAMATSU Si Photodiode for Direct Detection (S5377-0052(X))

[7] G. Pasquali et al., Nucl. Instr. Meth. A 301(1991) 101

[8] 3M Vikuiti^{TM} ESR foil, recommended by the crystal manufacturer

[9] http://www-linux.gsi.de/~weick/atima

[10] Z. Sosin et al., to be published

[11] CAEN V1724 digitizer

[12] http://www.gsi.de/informationen/wti/ee/elekt_entwicklung/triva_e.html

[13] RIO4-8072RE, CES, www.ces.ch

[14] http://www-win.gsi.de/daq/

[15] G.F. Knoll, "Radiation Detection and Measurement", 4-th ed., Chapt. 9, 16.

[16] C.A.J. Ammerlaan et al., Nucl. Instr. Meth. 22 (1963) 189; M. Pârlog et al., Nucl. Instr. Meth. A 613 (2010) 290; Z. Sosin, pivate comm., and to be published.

[17] G. Pausch et al., Nucl. Instr. and Meth. A 365 (1995) 176; L. Bardelli et al., Nucl. Instr. and Meth. A 654 (2011) 272